

Thermal compression of two-dimensional atomic hydrogen to quantum degeneracy

S. Vasilyev,¹ J. Järvinen,¹ A.I. Safonov,² and S. Jaakkola¹

¹*Wihuri Physical Laboratory, Department of Physics,
University of Turku, 20014 Turku, Finland*

²*Laboratory of Metastable Quantum Systems, ISSSP,
RRC Kurchatov Institute, 123182 Moscow, Russia*

(Dated: November 20, 2018)

We describe experiments where 2D atomic hydrogen gas is compressed thermally at a small "cold spot" on the surface of superfluid helium and detected directly with electron-spin resonance. We reach surface densities up to $5 \times 10^{12} \text{ cm}^{-2}$ at temperatures $\approx 100 \text{ mK}$ corresponding to the maximum 2D phase-space density ≈ 1.5 . By independent measurements of the surface density and its decay rate we make the first direct determination of the three-body recombination rate constant and get the upper bound $L_{3b} \lesssim 2 \times 10^{-25} \text{ cm}^4/\text{s}$ which is an order of magnitude smaller than previously reported experimental results.

PACS numbers: 05.30.Jp, 67.65.+z, 82.20.Pm

When adsorbed on the surface of superfluid helium spin-polarized atomic hydrogen ($\text{H}\downarrow$) is an ideal realization of a two-dimensional (2D) boson gas [1]. Helium provides a translationally invariant substrate and its surface-normal potential supports only one bound state for hydrogen with the binding energy $E_a=1.14(1) \text{ K}$ [2]. Even for such a weak interaction, lowering the surface temperature T_s well below 1 K leads to a large adsorbate density σ . At high $\text{H}\downarrow$ coverages three-body recombination is expected to be the dominant density decay mechanism setting the main obstacle to the achievement of the quantum degeneracy regime, where the thermal de Broglie wavelength Λ is larger than the average interatomic spacing. Degenerate 2D $\text{H}\downarrow$ is expected to exhibit collective phenomena such as the Kosterlitz-Thouless superfluidity transition and the formation of a quasicondensate.

Two methods of local compression of adsorbed $\text{H}\downarrow$ have been employed to overcome limitations caused by recombination and its heat. Magnetic compression has been successfully used to achieve quantum degeneracy [3, 4]. In this method the recombination heat is removed from the compressed $\text{H}\downarrow$ by ripplons of the helium surface and the cooling efficiency depends on the length of the heat transfer path. By decreasing the size of the compressed region to $20 \mu\text{m}$ we were able to achieve $\sigma\Lambda^2 \approx 9$ [3]. However, the small size of the sample together with large magnetic field gradients did not allow to implement direct diagnostics of adsorbed $\text{H}\downarrow$. In the thermal compression method [5, 6] cooling a small part of the sample cell wall well below the temperature of the rest of the wall leads to an exponential increase of σ on such a "cold spot". In this method the recombination heat is transferred from the ripplons to the phonons of helium [7] and then to the substrate beneath the spot. Therefore a larger spot is preferable as long as the total recombination rate on the spot becomes a limitation. The larger sample size and the homogeneity of the magnetic field make thermal compression better suited for direct studies of adsorbed

$\text{H}\downarrow$.

In the present work we use sensitive electron-spin resonance [8] to diagnose 2D $\text{H}\downarrow$ gas thermally compressed to $\sigma\Lambda^2 \approx 1.5$ and discuss the limitations and possible improvements of the "cold spot" method to reach and detect the Kosterlitz-Thouless transition. By independent measurements of the recombination rate and the surface density we obtain the first directly determined value, actually an upper bound, of the three-body surface recombination rate constant $L_{3b} \lesssim 2 \times 10^{-25} \text{ cm}^4/\text{sec}$. This is 4...10 times smaller than the earlier values measured indirectly [3, 9, 10, 11].

Our experimental setup is shown in Fig.1. The sample cell has been described elsewhere [8]. The low-temperature part of the ESR spectrometer, operating now as a mm-wave bridge, has been modified so that we may use three times smaller excitation powers and thus avoid ESR instability effects [8] in a wider temperatures range. Gradient coils were built to reduce the field inhomogeneity of the main magnet so that the width of the bulk line is decreased to $\approx 0.1 \text{ G}$. It has been found that even very small ($\leq 1 \text{ ppb}$) ^3He impurity in our isotopically purified ^4He condensed into the cell may significantly influence the adsorption of the 2D hydrogen [2]. Therefore we built an *in situ* helium film purifier, a reservoir with the large surface area of $2 \times 10^3 \text{ cm}^2$ located in zero field (Fig.1). Being cooled down to the lowest temperatures attained here the purifier adsorbs the remainder of ^3He atoms from the cell. The miniature RuO_2 thermometers used to measure the temperatures of the cell, the buffer volume and the $^3\text{He}/^4\text{He}$ coolant of the cold spot were calibrated to an accuracy better than 1 mK with a ^3He melting curve thermometer.

In a typical experiment we fill the cell and the buffer with atomic hydrogen from a low-temperature dissociator to a density $n \approx 10^{15} \text{ cm}^{-3}$. After switching off the discharge we stabilize the buffer to $T_b = 350 \text{ mK}$, the optimum temperature for getting the longest lifetime for

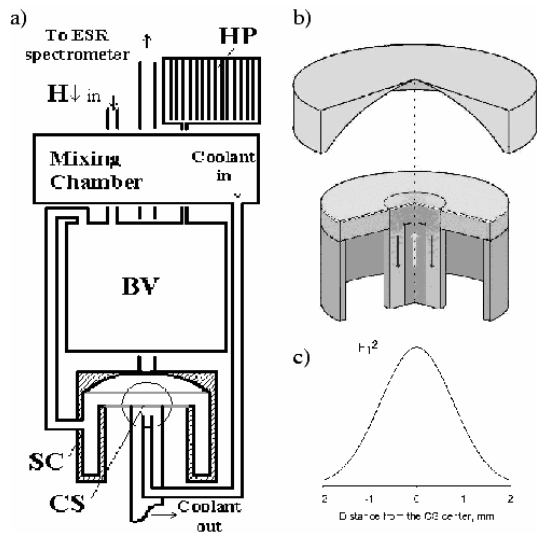


FIG. 1: (a) Scheme of the cell. SC = sample cell, CS = cold spot, BV = buffer volume, HP = helium purifier; (b) Fabry-Perot resonator with the cold spot in the center of its flat mirror; (c) Microwave field profile on the cold spot.

the hydrogen sample, and cool the cell to a desired temperature $T_c=60\dots170$ mK. The temperatures of the mixing chamber of the dilution refrigerator and the ^3He - ^4He stream cooling the cold spot (cp. Fig.1) are stabilized in the range $T_L=30\dots150$ mK. Thermal compression can be rapidly (< 5 s) turned on and off by changing the coolant temperature. Decays of our $\text{H}\downarrow$ samples were governed by impurity relaxation from “pure” hyperfine state b to more reactive state a [12]. To decrease the relaxation rate the cell is made of nonmagnetic materials (ultrapure copper, epoxy, Kapton foils) and its walls are coated at low temperatures with a 10..50 nm thick solid H_2 layer by running the dissociator for several days. The 0.2 cm diameter tube connecting the buffer and the cell is wide enough to render the exchange of atoms between the two volumes faster than the decay rates. This ensures a dynamic density equilibrium between the volumes. Decays of $\text{H}\downarrow$ samples were monitored at fixed temperatures of the cell region. Recombination rates in the buffer and cell are measured calorimetrically from the feedback powers of the respective temperature controllers. We find that at the present temperatures the loss rate of atoms in the buffer is negligible compared to that in the cell. Integrating the latter we extract the bulk densities as functions of time in both volumes.

The evolution of the ESR spectrum during the decay of a $\text{H}\downarrow$ sample is shown in Fig. 2. The resonance line originating from the adsorbed atoms is shifted from the bulk line due to the non-zero average dipolar field in this 2D system [8, 13]. To find the surface density we integrate the surface and bulk absorption ESR lines. The bulk integral is calibrated calorimetrically against the absolute value of the bulk density, which method does

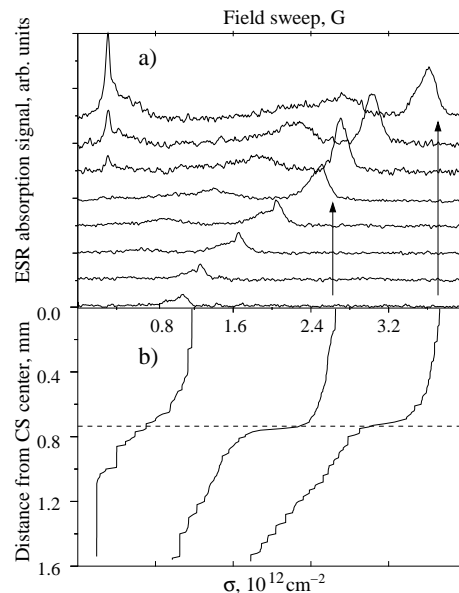


FIG. 2: Evolution of (a) $\text{H}\downarrow$ ESR spectrum and (b) surface density profile during the decay of a $\text{H}\downarrow$ sample. The traces were recorded at intervals of 500 s at $T_L = 45$ mK and $T_c = 112$ mK. The dashed line marks the edge of the cold spot.

not rely on the adsorption isotherm and yields the absolute value of surface density with an accuracy of 10%. With this method we checked the relation between the internal dipolar field and the surface density and found $\Delta H_d = A\sigma$, where $A = 1.05(10) \times 10^{-12}$ G cm 2 . This direct and more accurate measurement agrees well with the previous experimental and calculated results [8, 13].

The ESR lineshape of adsorbed atoms $S(h)$ as a function of magnetic field sweep h is broadened due to the inhomogeneity of the temperature $T_s(r)$ and, consequently, density $\sigma(r)$ of the 2D gas in the spot region. It is given by the relation

$$S(h) \sim \int H_1^2(r) f_i(h - A\sigma(r)) \sigma(r) r dr, \quad (1)$$

where $H_1^2(r)$ is the microwave field profile on the flat mirror. The intrinsic lineshape $f_i(h)$ of the adsorbed atoms is very narrow [8] and can be replaced by a delta function. We used Eq. (1) to extract density profiles $\sigma(r)$ from the observed lineshapes using a numerical fitting routine. Examples of the surface density profiles recovered for a few ESR spectra is presented in Fig. 2b. Even for the largest temperature difference between the cell and spot the surface density is homogeneous within 10% on the cold spot. The relatively slow decrease of σ outside the spot ($r > 0.75$ cm) gives rise to a broad maximum between the bulk and main surface signals.

Numerous decays have been measured at various cell and spot temperatures. Plots of the maximum surface density as a function of the bulk density n for a fixed $T_c=154$ mK and various coolant temperatures T_L are pre-

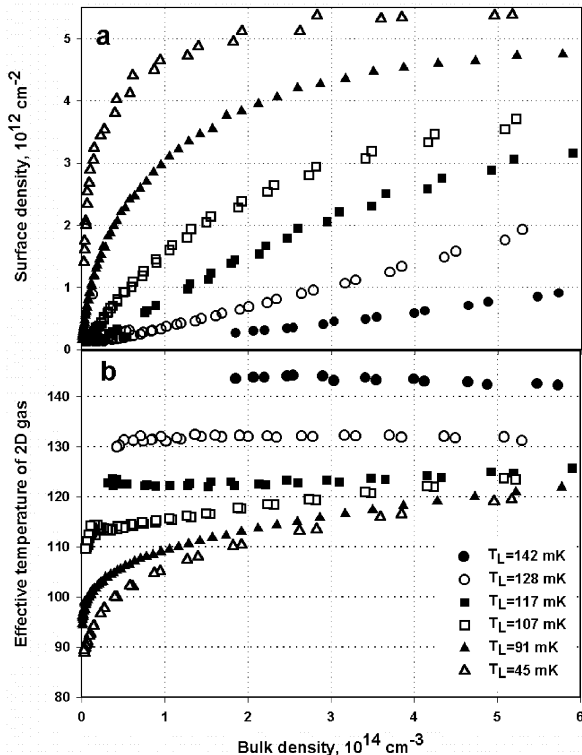


FIG. 3: (a) Maximum surface density on the cold spot for $T_C=154$ mK and various T_L . (b) Effective surface temperatures T_s calculated using adsorption isotherm.

sented in Fig. 3a. For low bulk densities the surface density increases linearly with n , as it should do according to the adsorption isotherm [5, 14]. Effective temperature of the 2D gas T_s (Fig. 3b) is extracted from the σ and n values using the adsorption isotherm and taking $E_a=1.14(1)$ K [2]. At high temperatures $T_L \gtrsim 100$ mK and small differences $T_L - T_c \lesssim 10$ mK, T_s turns out be equal to T_L within 1 mK, the error bar of our thermometry. This coincidence is regarded as a confirmation of the above mentioned adsorption energy value.

The observed levelling of σ with increasing n (upper plots in Fig. 3) points to an overheating of the 2D $\text{H}\downarrow$ gas which begins the earlier the lower is the coolant temperature. The surface temperatures T_s extracted from the low-density parts of the curves start to exceed the coolant temperature, the difference increasing with increasing $T_c - T_L$. This may be explained by heating of the spot by a heat flux from the much warmer cell walls. Another possible reason for the saturation of the surface density could be a 2D hydrodynamic flow of $\text{H}\downarrow$ on the spot out of the high density region. If the flow becomes fast enough, the balance between the adsorption and desorption rates will be disturbed. Interaction of $\text{H}\downarrow$ with surface quasiparticles like ripples and ^3He impurities should impede the flow. To distinguish between

the roles of the overheating and the 2D flow we added ^3He into the cell varying the ^3He surface density up to 10^{14} cm^{-2} . This did not help to get any higher density for the adsorbed $\text{H}\downarrow$. On the other hand, the maximum σ appeared to be very sensitive to the rate of one-body impurity relaxation in the cell and buffer. Therefore we conclude that the recombination overheating is more important than the 2D flow and limits the highest achieved densities. The T_s values extracted from the adsorption isotherm (Fig. 3) can be considered as good upper limits to the real surface temperatures.

In our experiments the decay of $\text{H}\downarrow$ is determined mainly by one-body relaxation and three-body recombination on the cell walls. Due to the density profile over the spot at high σ being nearly step-like (Fig. 2) we can separate the spot contribution and write for the total recombination rate

$$\frac{dN}{dt} = -(2G_1\sigma + L_{3b}\sigma^3)A_{cs} - R(n, T_c, T_b), \quad (2)$$

where G_1 is the one-body relaxation rate constant, L_{3b} the three-body recombination rate constant, A_{cs} the cold spot surface area and $R(n, T_c, T_b)$ is the atom loss rate in the rest of the cell and the buffer. We tried to extract the spot contribution by monitoring recombination powers during decays at different coolant temperatures and keeping conditions in the rest of the cell region unchanged. No difference was found within the noise of the temperature controller signal indicating that the spot contribution is very small compared to that of the rest of the walls. Therefore, to get a higher resolution, we used the possibility to turn the spot cooling rapidly on (or off) during the decay (Fig. 4) and performed such experiments at various cell temperatures and bulk densities. Even for the largest change in the surface density of the spot the corresponding change of the total recombination power in the cell was hardly discernible from the noise. Assuming that three-body recombination is the dominant loss mechanism on the spot and integrating the three-body rate over the actual density profile of the spot we extract the upper limit $L_{3b} \leq 2 \times 10^{-25} \text{ cm}^4/\text{s}$. This is the first directly measured value based on independent determinations of the recombination rate and surface density. It agrees well with the calculations of de Goey et al. [15], but is an order of magnitude lower than the L_{3b} values reported in several previous works [9, 10, 11].

In all previous measurements of surface recombination σ was inferred into the rate equations through the adsorption isotherm. Instead of Eq. (2) a rate equation for the bulk density

$$\frac{dn}{dt} = -G_1^e n - L_{3b}^e n^3, \quad (3)$$

was used. Here $G_1^e = G_1(A/V)\Lambda \exp(E_a/T_s)$ and $L_{3b}^e = L_{3b}(A/V)\Lambda^3 \exp(3E_a/T_s)$ are effective rate constants with A/V being the area-to-volume ratio of the

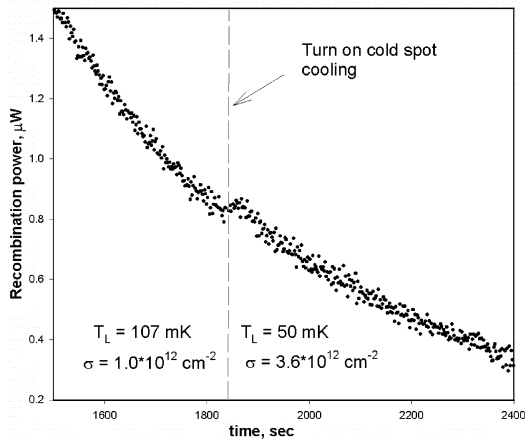


FIG. 4: Change in recombination power when the temperature of the cold spot is rapidly decreased from 107 to 50 mK and the surface density increases from $1 \times 10^{12} \text{ cm}^{-2}$ to $3.6 \times 10^{12} \text{ cm}^{-2}$.

cell. The effective constants were extracted from the fits of the measured $n(t)$ curves and the adsorption energy and the intrinsic constants G_1 and L_{3b} were obtained from the Arrhenius plots of the effective constants. There are however two fundamental drawbacks in this approach. First, E_a and the intrinsic rate constants are correlated parameters, and even a small uncertainty in E_a can seriously affect the accuracy of the intrinsic constants. A ^3He content as small as 0.1 ppm can be a reason for some of the published values of E_a being $\approx 10\%$ lower than the latest value $E_a = 1.14(1) \text{ K}$ obtained for isotopically purified ^4He [2] and confirmed also in this work. At $T_s \approx 100 \text{ mK}$ this error decreases the factor $\exp(3E_a/T_s)$ and increases L_{3b} by an order of magnitude. Another problem arises from the uncertainty of T_s due to the recombination heating of the 2D gas. This makes the surface temperature a function of time in the decays and does not allow to use Eq. (3) with G_1^c and L_{3b}^c being constant. In the present method we do not rely on the adsorption isotherm, but the error in L_{3b} is determined only by the absolute inaccuracy of σ and is at most 30%.

Appearance of a superfluid 2D $\text{H}\downarrow$ on the cold spot is expected to manifest itself as an abrupt change of the density profile and ESR lineshape. In this work superfluidity was not yet observed. The highest surface density $\sigma \approx 5 \times 10^{12} \text{ cm}^{-2}$ was achieved at $T_s \approx 100 \text{ mK}$ corresponding to the quantum degeneracy degree of about 1.5. Lowering the temperature of the sample cell below 110 mK or increasing the bulk density above $n \approx 2 \times 10^{14} \text{ cm}^{-2}$ was found to excessively increase the recombination rate on the cell walls thus overheating the 2D $\text{H}\downarrow$ on the cold spot. On the other hand, when the cell walls were warmer than 150 mK we could not cool the spot sufficiently due to a heat flux through the spot substrate and thermal accommodation of the atoms from the bulk. When

designing the cell, three-body recombination on the spot was thought to be faster than what it turned out to be and this was the reason to limit the spot size. However, one-body surface relaxation outside the spot was observed to give the dominant contribution to the decay of the sample and appeared to be the main limitation in the present experiments. We succeeded in decreasing the rate of one-body relaxation to $G_1 \approx 7 \times 10^{-2} \text{ s}^{-1}$ at $T_c \approx 100 \text{ mK}$, smallest ever reported in $\text{H}\downarrow$ experiments [4, 9, 10, 11]. Yet in future experiments one should find a way to reduce the G_1 even further, e.g., by covering the cell walls with a diamagnetic insulating material [14]. Another modification to get higher surface densities and to make the study of surface recombination more quantitative would be to make the cold spot larger and thermally better insulated from the cell. On the basis of the upper limit for L_{3b} obtained in the present work we estimate that such modifications would result in an increase of the degeneracy parameter $\sigma\Lambda^2 \gtrsim 3$, where the three-body recombination probability starts to decrease due to quantum correlation effects [3].

We thank I.I. Lukashevich and A.A. Kharitonov for collaboration. This work was supported by the Academy of Finland, Wihuri Foundation, INTAS, the Russian Ministry of Industry, Science and Technology and the RFBR.

* Electronic address: servas@utu.fi

- [1] For a review, see J. T. M. Walraven, in *Fundamental Systems in Quantum Optics*, edited by J. Dalibard, J. M. Raimond, and J. Zinn-Justin (Elsevier, Amsterdam, 1992), p. 485.
- [2] A. I. Safonov et al., Phys. Rev. Lett. **86**, 3356 (2001).
- [3] A. I. Safonov, S. A. Vasilyev, I. S. Yasnikov, I. I. Lukashevich, and S. Jaakkola, Phys. Rev. Lett. **81**, 4545 (1998).
- [4] A. P. Mosk, M. W. Reynolds, T. W. Hijmans, and J. T. M. Walraven, Phys. Rev. Lett. **198**, 4440 (1998).
- [5] B. V. Svistunov, T. W. Hijmans, G. V. Shlyapnikov, and J. T. M. Walraven, Phys. Rev. B **43**, 13412 (1991).
- [6] A. Matsubara et al., Physica B **194-196**, 899 (1994).
- [7] M. W. Reynolds, I. D. Setija, and G. V. Shlyapnikov, Phys. Rev. B **46**, 575 (1992).
- [8] S. A. Vasilyev et al., Phys. Rev. Lett. **89**, 153002 (2002).
- [9] R. Sprik, J. T. M. Walraven, G. H. van Yperen, and I. Silvera, Phys. Rev. B **34**, 1986 (1986).
- [10] D. A. Bell et al., Phys. Rev. B **34**, 7670 (1986).
- [11] M. W. Reynolds et al., Phys. Rev. B **31**, 7503 (1985).
- [12] I. F. Silvera and J. T. M. Walraven, *Progress in Low Temperature Physics*, vol. X (North-Holland, Amsterdam, 1986), p. 139.
- [13] I. Shinkoda and W. N. Hardy, J. Low Temp. Phys. **85**, 99 (1991).
- [14] A. P. Mosk, Ph.D. thesis, University of Amsterdam (1999).
- [15] L. P. H. de Goey, J. P. J. Driessen, B. J. Verhaar, and J. T. M. Walraven, Phys. Rev. Lett. **53**, 1919 (1984).